

Monotonic and Cyclic Tensile Properties of ABS Components Fabricated by Additive Manufacturing

C. W. Ziemian^a, D. E. Cipoletti^a, S. N. Ziemian^b, M. N. Okwara^c, K. V. Haile^a

^aDepartment of Mechanical Engineering, Bucknell University, Lewisburg, PA 17837

^bDepartment of Biomedical Engineering, Duke University, Durham, NC 27705

^cDepartment of Chemical Engineering, Bucknell University, Lewisburg, PA 17837

REVIEWED

Abstract

An investigation of tensile strength and cyclic tension-tension fatigue behavior has been performed on layered ABS components fabricated by fused deposition modeling (FDM). Experimentation was designed to focus specifically on the effect of specimen mesostructure on monotonic tensile behavior and tensile-fatigue life. Analyzed mesostructures include unidirectional laminae with parallel fiber orientations ranging from $\theta = 0^\circ$ (aligned with the loading axis) to $\theta = 90^\circ$ (perpendicular to the loading axis), and alternating laminae with a layering pattern of $\theta^\circ/(\theta-90^\circ)$ fiber orientations. The unidirectional 0° specimens achieved the greatest tensile strength and effective elastic modulus, while the alternating $+45^\circ/-45^\circ$ specimens displayed the best fatigue performance of the specimens tested. Results highlight the anisotropic behavior of FDM components and suggest that the tensile behavior is improved by aligning the fibers of unidirectional laminae more closely with the axis of the applied stress. In addition, the specimens with $\theta^\circ/(\theta-90^\circ)$ fiber orientations displayed incrementally improved tensile properties and fatigue performance from an apparent offsetting effect that results from alternating laminae. The fracture surfaces of the specimens were analyzed using scanning electron microscopy in order to gain further insights into the fatigue damage and failure mechanisms.

1. Introduction

Fabrication by additive manufacturing (AM) processes begins with a computerized solid model of the desired object. This model is then tessellated and mathematically sliced into a series of parallel cross-sections or layers. A machine traverse path is then generated for the creation of each of these layers or laminae. The physical part is then fabricated from the bottom-most layer upward, by incrementally building one model slice on top of the previously built layer. With the assistance of any needed support structures, this additive layering process is capable of fabricating components with complex geometrical shapes in a single setup without tooling or human intervention.

Although originally used for rapid prototyping, AM processes have more recently begun to evolve into rapid manufacturing methods intended to produce functional components for end use in marketable products [1]. This advancement requires that mechanical properties of AM components sufficiently meet in-service loading and operational requirements, and are reasonably comparable to the properties of parts produced by more traditional manufacturing techniques. It is subsequently essential that a thorough understanding of the mechanical

properties and behavior of AM parts exists, and that these properties can be accurately predicted and controlled.

Fused deposition modeling (FDM) is an AM process that produces durable components by layering extruded materials; most commonly acrylonitrile butadiene styrene (ABS) plastic. The FDM process (Figure 1) involves the partial melting and extrusion of a flexible ABS filament through a heated nozzle, forming a thin, single layer pattern on the surface of the previously extruded layer. Each resulting layer (or lamina) is thus composed of closely packed, parallel, semi-solid fibers or rasters that subsequently cool, solidify, and bond with adjacent and previously deposited fibers. FDM components formed in this manner have been shown to possess anisotropic mechanical properties. The literature includes considerable attention to the subsequent directional dependence of the mechanical properties of FDM components, including investigations of tension, compression, flexural, and impact strengths. Although not a comprehensive review, consideration of several such works is presented here.

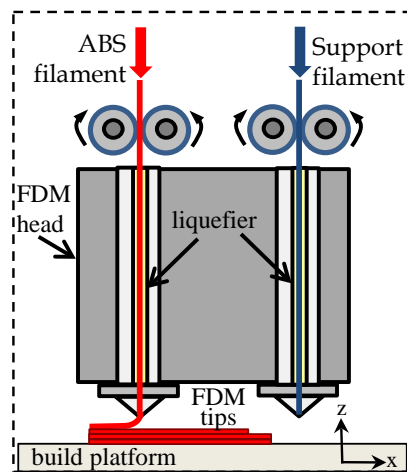


Figure 1. Schematic of the FDM process

Rodriguez et al. [2,3] investigated the tensile strength of FDM specimens with varying fiber orientations and found that strength was maximized by aligning the fibers with the axis of the tension force. Ahn et al. [4] utilized a factorial experiment to define the effects of model temperature, bead width, raster orientation, air gap, and ABS color on both tensile and compressive strengths of FDM parts. Their study determined that air gap and raster orientation affected tensile strength, while compressive strength was not affected by these factors. A similar investigation completed by Sood et al. [5] varied the layer thickness, build orientation, raster angle, raster width, and air gap. These researchers analyzed the functional relationship between process parameters and tensile strength using response surface methodology, and results indicated the importance of the bonding and distortion within the part. On the basis of this work, Sood et al. [6] further examined the effect of these process parameters on the compressive strength of FDM specimens. Their work developed a statistically validated predictive equation, and further highlights the importance of fiber-to-fiber bond strength and the control of distortion. Lee et al. [7] concluded that layer thickness, raster angle, and air gap all significantly influence the elastic performance of compliant FDM-ABS prototypes. A study conducted by Es Said et al.

[8] analyzed the issue of volumetric shrinkage and raster orientation with respect to tensile, flexural and impact strengths. Ziemian et al. [9] completed a comprehensive experimental study of the tensile, compressive, flexural, and impact properties of FDM parts with varying raster orientations, and compared results with those obtained for injection molded parts made of the same FDM-ABS material. Their study further emphasized the anisotropic behavior of FDM specimens subjected to tensile, bending, and impact forces, with more limited directional dependency seen for parts subjected to compression.

The abovementioned studies reveal the directional dependence of the mechanical properties of FDM parts as a result of mesostructure and fiber-to-fiber bond strength, and provide numerous insights and recommendations regarding significant process parameters and the development of component build rules. An important factor still limiting the use of FDM components within functional parts, however, is the remaining question of their fatigue response. There is currently limited work published with regard to the cyclical fatigue performance of FDM components. Lee and Huang [10] completed an investigation that analyzed the total strain energy absorbed by two different FDM plastics during fatigue testing. While their work provides important baseline information, their experiment tested only one material specimen at each stress level, thereby precluding any statement of the statistical significance of results. Similarly, Ziemian et al. [9] completed a preliminary study of the fatigue properties of FDM components as part of an experimental investigation focused on the dependence of the tensile, compressive, impact, and bending strengths on raster orientation, i.e. the direction of the polymer beads relative to the loading direction of the part. The fatigue study included a statistical sample of each of four raster orientations, but was limited to the consideration of only one stress level.

The work presented here represents an expansion of the previous studies completed by Ziemian et al. [9, 16] to include a more comprehensive investigation of monotonic tension and cyclical tension-tension fatigue behavior of FDM specimens with varying meso-structures. Statistical samples were studied with multiple raster orientations and stress levels. Results were examined and interpreted with respect to the microscopic failure mechanisms identified by scanning electron microscopy (SEM).

2. Experimental Approach and Methods

2.1 Specimen Construction

Dogbone shaped specimens, per the ASTM D638 standard [11], were fabricated on a Stratasys Vantage-i machine of acrylonitrile butadiene styrene (ABS-P400 Stratasys®). Specimens were all built lying flat on the machine platform, with the minimum part dimension aligned with the z-axis of the machine (Figure 2a). A T12 nozzle was used. FDM machine process parameters were set at default or recommended values, including air gap (0.0 mm), road width (0.3048 mm), slice height (0.1778 mm), interior fill style (solid normal), and part fill style (perimeter/raster). Each piece had a z-height, or specimen thickness, of 2.54 mm and included a total of 15 total layers. Parts were built in a total of ten different fiber orientations. Raster or fiber angles, as defined with respect to the longitudinal x-axis, included unidirectional laminates (15 identical layers) of 0°, 15°, 30°, 45°, 60°, 75°, and 90°, and alternating laminates of +15°/-75°, +30°/-60°, and +45°/-45°. Several representative orientations are displayed in Figure 2b.

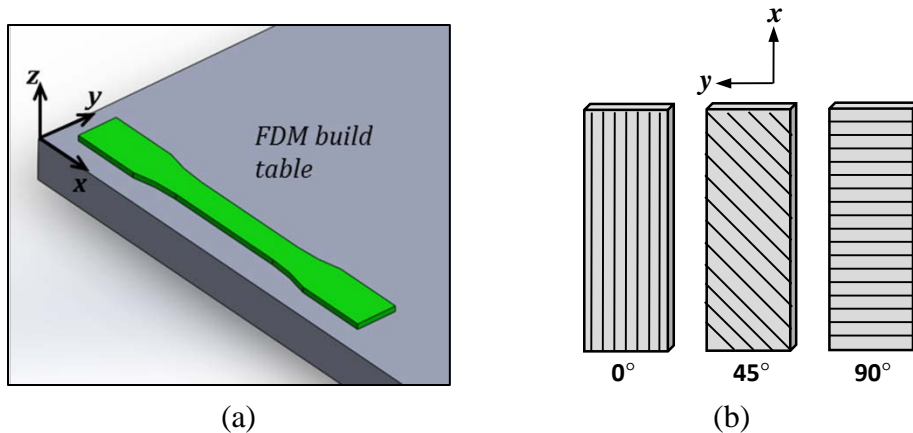


Figure 2. (a) FDM build orientation, and (b) several representative fiber orientations.

Single ABS-400 fibers and injection molded specimens were also tested to allow for the comparison of the tensile behavior of the ABS filament material in non-layered forms. For the injection molded specimens, the FDM-ABS filament was fed into a polymer granulator and cut into pellets that were then melted in a Morgan Press G-100T. Molding was done using a nozzle temperature of 270 °C, mold preheat temperature of 120° C, clamping force of 71 kN, and injection pressure of 41 MPa.

2.2 Mechanical Testing

Tension tests were first completed, per the ASTM D638 standard [11], in order to determine the mean ultimate tensile stress (UTS), yield stress, and effective modulus of elasticity along the longitudinal loading direction for each of the ten different raster orientations. Four specimens of each of the ten orientations (40 total) were tested on an Instron dual column uniaxial material testing machine with .057 micron displacement precision, up to 0.001 N force accuracy, and 10kN load capacity. Tests were run at a strain rate of 0.00065 s⁻¹, with an associated grip speed of 4.46 mm/min. Each tension specimen was pulled until fracture occurred. Additional 0° and 90° specimens were affixed with strain gages to record lateral and transverse strains during tension testing, from which major and minor Poisson's ratios were estimated.

Tension-tension fatigue tests were performed according to a 4² factorial experimental design, with two factors analyzed at 4 levels each, i.e. 16 total treatment combinations. Factor **A**, raster orientation, included 0°, 45°, 90°, ±45°. Factor **B**, maximum stress level, included 90, 75, 60, and 45% of UTS. The minimum cycle load in each case was 1/10 of the maximum load (stress ratio $R = 0.1$), and tests were performed with triangular load variation in time. The testing was completed in accordance with the ASTM D7791 standard [12], with at least four replicates tested for each factor combination. Testing was performed at room temperature in a humidity-controlled environment using a low frequency (0.25 Hz) to limit the possibility of localized heating due to hysteresis, and a runout value of 25 hours of testing, or approximately 17,500 cycles.

2.3 Statistical Data Analysis

Comparisons of the mean values of the UTS, yield stress, Young's modulus, and fatigue life of the different specimen types were made using a fixed-effects model of analysis of variance (ANOVA) [13]. A one-way ANOVA was used to assess the effect of the specimen mesostructure, i.e. raster orientations and unidirectional or alternating laminae, on the different response variables resulting from tensile tests in order to assess the level of anisotropic behavior. A two-way ANOVA was completed to evaluate the equivalence of the mean number of cycles to failure for the treatment factors of specimen mesostructure and maximum fatigue stress level (90%, 75%, and 60% of UTS).

2.4 Microscopic Evaluation

The fracture surfaces that resulted from tension and fatigue testing were subsequently prepared by gold sputtering and inspected using a JSM 500-type JEOL scanning electron microscope (SEM). An Olympus GX-Series optical microscope was also used to take low magnification images of specimen cross sections in order to estimate the load-bearing area of each of the specimen types tested.

3. Data Results

3.1 Tension Tests

A summary of the tensile strength and modulus data for the tested specimens is presented in Table 1. The elastic modulus for each specimen was calculated from the slope of the linear portion of the stress-strain curves, i.e. $\Delta\sigma/\Delta\varepsilon$. In this study, a MATLAB program was written to perform a least squares linear regression on the data and determine the effective modulus for each specimen. While the single fiber and injection molded specimens were the strongest and stiffest overall, the data for the FDM components indicate that the mean ultimate and yield strengths (0.2% offset) and Young's modulus were largest for the longitudinal (0°) specimens and smallest for the 60° , 75° , and 90° specimens. The mean UTS of the 60° , 75° , and 90° specimens was found to be only 36.3% of that of the 0° fiber specimens, and the mean elastic modulus of the 60° , 75° , and 90° specimens was 60.6% of mean effective E for the 0° fiber specimens. A graphical display of the relative differences in the computed E values is seen in Figure 3 for several representative specimens.

A one-way ANOVA [13] was used to compare the mean UTS and effective elastic moduli values associated with the different specimen mesostructures tested. The results indicated a statistically significant difference between both the UTS values and the moduli of the tested unidirectional laminate specimens. At a level of significance of $\alpha = 0.05$, the calculated F -test statistics were $F(6,28) = 1261.25$ for the UTS analysis and $F(6,28) = 528.18$ for the moduli analysis. In both cases, the p -value were < 0.001 , suggesting that tensile strength and effective moduli are affected by the layered processing and the subsequent directionality of the polymer molecules. Additional post hoc Tukey analyses [13] specified that these difference were significant (at $\alpha = 0.05$) for all pairwise comparisons of the UTS and moduli of the unidirectional laminates except for those between the 60° , 75° , and 90° specimens (Table 2). Similarly, ANOVA and post hoc analyses indicated that the differences between all pairwise

comparisons of mean UTS and moduli values of the $\theta^\circ/(\theta-90^\circ)$ laminates were significant except for that between the mean UTS of the $+15^\circ/-75^\circ$ and $+30^\circ/-60^\circ$ specimens.

Table 1. Tension test results for ten different raster orientations, injection molded, and single fiber specimens tested; Standard deviations in parentheses;

Fiber Orientation	Mean Yield Strength (MPa)	Mean Ultimate Strength (MPa)	Mean Elastic Modulus (MPa)
0°	22.82 (0.36)	23.08 (0.30)	1820.54 (15.41)
15°	15.53 (0.52)	15.82 (0.50)	1722.31 (20.47)
30°	13.26 (0.43)	13.99 (0.40)	1475.52 (41.40)
45°	10.06 (0.39)	10.61 (0.39)	1231.15 (28.43)
60°	8.04 (0.23)	8.50 (0.29)	1103.40 (33.77)
75°	7.67 (0.16)	7.97 (0.30)	1105.64 (41.11)
90°	8.19 (0.18)	8.37 (0.31)	1103.24 (26.90)
+45°/-45°	14.53 (0.34)	15.71 (0.30)	1362.28 (19.97)
+15°/-75°	14.37 (0.24)	14.39 (0.25)	1524.28 (20.44)
+30°/-60°	14.17 (0.17)	14.67 (0.13)	1443.83 (44.58)
Injection Molded	26.32 (0.81)	27.00 (0.74)	1613.19 (60.94)
Single FDM fiber	25.14 (0.41)	27.74 (0.53)	1914.48 (43.23)

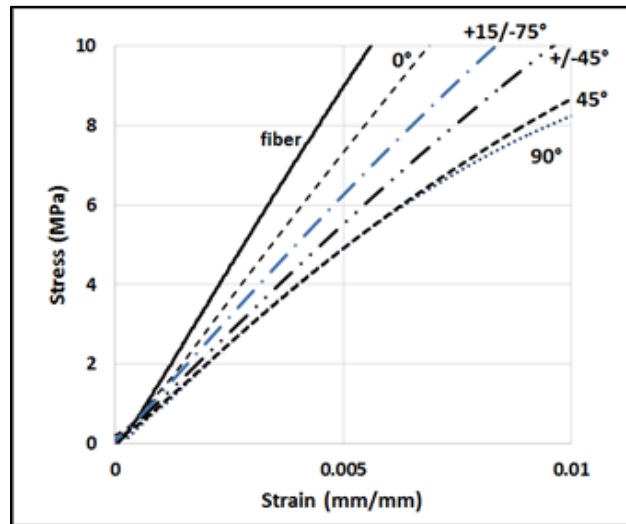


Figure 3. Magnification of the linear portion of the stress-strain curves for several representative FDM specimens;

A one-way ANOVA [13] was used to compare the mean UTS and effective elastic moduli values associated with the different specimen mesostructures tested. The results indicated a statistically significant difference between both the UTS values and the moduli of the tested unidirectional laminate specimens. At a level of significance of $\alpha = 0.05$, the calculated F -test statistics were $F(6,28) = 1261.25$ for the UTS analysis and $F(6,28) = 528.18$ for the moduli analysis. In both cases, the p -value were < 0.001 , suggesting that tensile strength and

effective moduli are affected by the layered processing and the subsequent directionality of the polymer molecules. Additional post hoc Tukey analyses [13] specified that these difference were significant (at $\alpha = 0.05$) for all pairwise comparisons of the UTS and moduli of the unidirectional laminates except for those between the 60°, 75°, and 90° specimens (Table 2). Similarly, ANOVA and post hoc analyses indicated that the differences between all pairwise comparisons of mean UTS and moduli values of the $\theta^\circ/(\theta-90^\circ)$ laminates were significant except for that between the mean UTS of the +15°/-75° and +30°/-60° specimens.

Table 2. Post hoc Tukey [13] multiple comparisons of mean UTS values for the unidirectional laminates tested

Fiber Orientation (i)	Fiber Orientation (j)	Difference of Mean UTS (i-j)	95% Confidence Interval	
			Lower Bound	Upper Bound
0°	15°	7.123	6.323	7.922
	30°	9.118	8.318	9.917
	45°	12.470	11.670	13.270
	60°	14.470	13.670	15.270
	75°	15.018	14.218	15.817
	90°	14.715	13.915	15.515
15°	30°	1.995	1.195	1.995
	45°	5.348	4.548	5.348
	60°	7.348	6.548	7.348
	75°	7.895	7.095	7.895
	90°	7.593	6.793	7.593
30°	45°	3.352	2.553	4.152
	60°	5.352	4.553	6.152
	75°	5.900	5.100	6.700
	90°	5.598	4.798	6.397
45°	60°	2.000	1.200	2.800
	75°	2.548	1.748	3.347
	90°	2.245	1.445	3.045
60°	75°	0.548*	-0.252	1.347
	90°	0.245*	-0.555	1.045
75°	90°	-0.303*	-1.102	0.497

* Mean difference is not significant at the 0.05 level

The monotonic tensile response observed for several specimen types is displayed in Figure 4. The stress-strain curves reveal dissimilarities with regard to both strength and fracture strain of the different raster orientations. The 45°, 60°, 75°, and 90° unidirectional specimens strained significantly less than the others, with only a small amount of deformation prior to failure, and fracture occurring almost immediately after yielding. These specimens also displayed considerably smaller tensile strengths than the 0°, 15°, and 30° specimens. These results suggest that the tensile responses of specimens with $\theta \geq 45^\circ$ fibers are highly dependent on the inter-fiber bond strength that forms during processing. The stress-strain curves for the injection molded and the 0° FDM specimens, in contrast, display much more significant straining prior to failure, and higher tensile strengths. They also exhibit a post yielding drop in stress that is symptomatic of the polymer chain stretching, rotation, and sliding in thermoplastic materials [10]. As anticipated, this suggests that the tensile response of the 0° specimens is based much

more significantly on the behavior of the ABS polymer and the extruded fibers themselves. Finally, the alternating $\theta^\circ/(\theta-90^\circ)$ specimens display levels of tensile strength and post-yield straining that are less than the $\theta \leq 15^\circ$ parts, but greater than the other unidirectional laminates.

Also of interest is the perceptible stepped shape of the 0° stress-strain curve seen in Figure 4. These specimens failed in the transverse direction with the progressive rupture of individual fibers occurring as they were stressed along their axial direction. Typically, several fibers broke on the outer surface of the specimen width, but the specimen continued to support load, albeit levelling off at a lower value of stress. The new smaller width created by this failure then generates a concentration of stress and becomes the location of the next fiber breakages. This progressive type of failure also included some degree of fiber pullout and delamination.

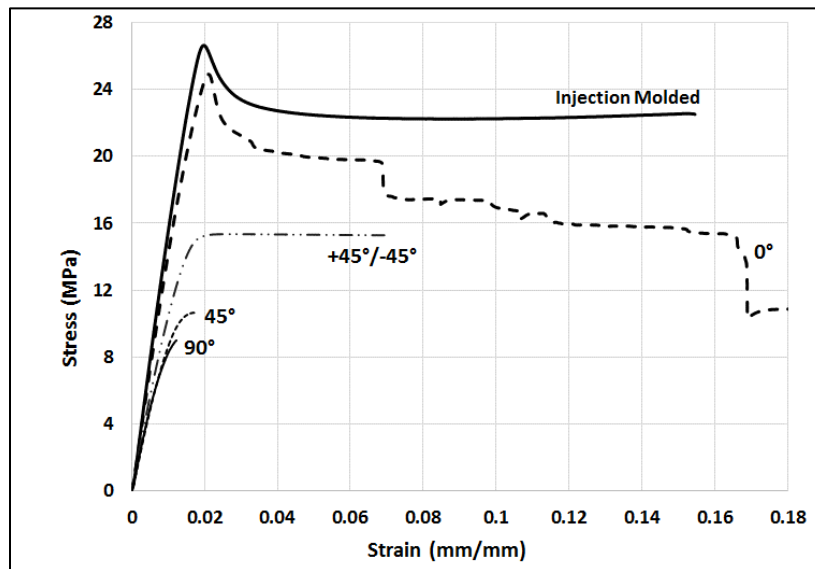


Figure 4. Stress versus strain curves of several representative specimens

3.2 Tension-Tension Fatigue Tests

The tension-tension fatigue results, summarized on the basis of normalized stress (% UTS) are presented in Table 3. Results indicate that of the four mesostructures tested, the unidirectional transverse (90°) raster specimens survived the shortest fatigue life and the specimens with alternating $+45^\circ/-45^\circ$ laminae had the longest fatigue life at each of the normalized stress levels. The S-N curves in Figure 5 highlight the fact that the 90° specimens fractured with the smallest mean number of cycles to failure at each of the tested stress levels. The next largest mean fatigue life was for the unidirectional laminae at 45° , then the 0° , and finally the alternating $+45^\circ/-45^\circ$ raster specimens, which survived the greatest number of cycles to failure at each of the normalized stress levels.

A two-way ANOVA revealed that the main effects of both stress level and fiber orientation are significant at a level of $\alpha = 0.05$ [13]. In addition, the stress*orientation interaction effect also proved to be significant, with a calculated F -test statistic of $F(6,36) = 24.05$ and a p -value of 0.000. These results suggest that the orientation of the ABS fibers

relative to the loading axis substantially affects the tension-fatigue properties of the FDM specimens, and the difference between the mean numbers of cycles to failure of each orientation is statistically significant at each stress level. The (stress level*fiber orientation) interaction effect further suggests that the relative influence of fiber orientation is different for each stress level, and vice-versa.

Table 3. Mean number of cycles to failure in tension-tension fatigue testing; Standard deviations in parentheses

Max % of UTS	Fiber Orientation			
	0°	45°	90°	+45/-45°
90	315 (39.2)	176 (39.8)	45 (13.9)	1155 (86.9)
75	1738 (161.7)	706 (149.9)	308 (193.2)	4593 (366.1)
60	4315 (591.3)	3057 (870.5)	1271 (228.8)	13628 (3463.2)
45	16419* (1149.7)	17843 (4230.0)	10575 (2757.7)	17366* [^] (54.6)

* Run at 50% UTS; [^] All 50% UTS default specimens were stopped (unbroken) at runout value of 25 hours;

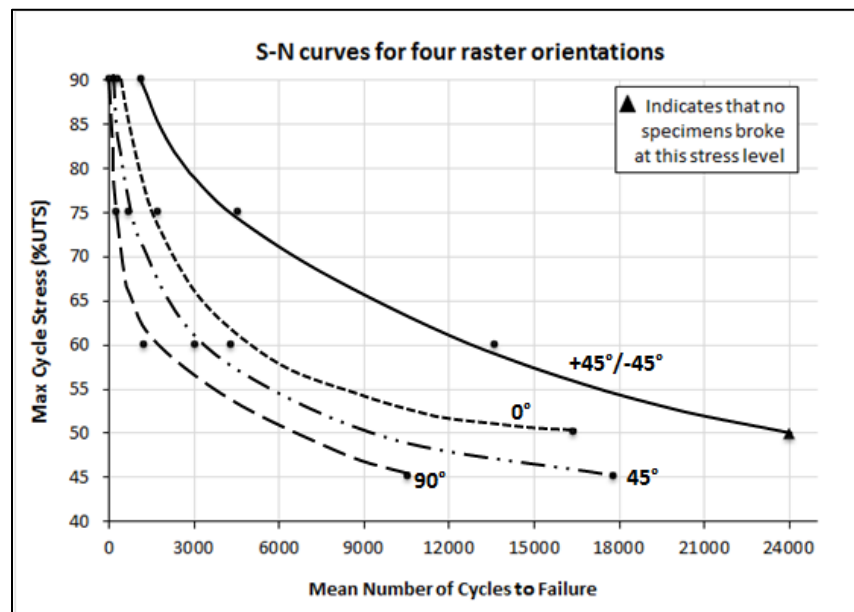


Figure 5. S-N curves for the four mesostructures that underwent fatigue testing

4. Specimen Inspection

4.1 Macroscopic Analysis

Inspection of the fractured specimens from both tension and fatigue testing highlights variation in the weakest path of crack propagation as a function of the orientation of the fibers. Fracture paths that are controlled by weak inter-fiber bonding are affected by the residual stresses that result from the volumetric shrinkage of the polymer laminates during solidification and cooling [14]. This was found to be the case for the unidirectional specimens with $15^\circ \leq \theta \leq$

90°, which consistently failed along the bond between the fibers (Figure 6a). The $\theta^\circ/(90-\theta^\circ)$ specimens, in contrast, displayed intersecting fracture paths along the two fiber directions, creating the appearance of a saw-tooth fracture surface across the specimen width (Figure 6b). The 0° specimens presented the most erratic fracture paths on a macro scale as a result of the failure behavior experienced. Most 0° specimens started to fracture as individual fibers first broke on the outermost surface of the width. The specimens would then continue to support load, with individual fibers breaking intermittently, until full fracture eventually occurred (Figure 6c). This behavior is also evident in the stepped shape of the 0° stress-strain curve presented in Figure 4.

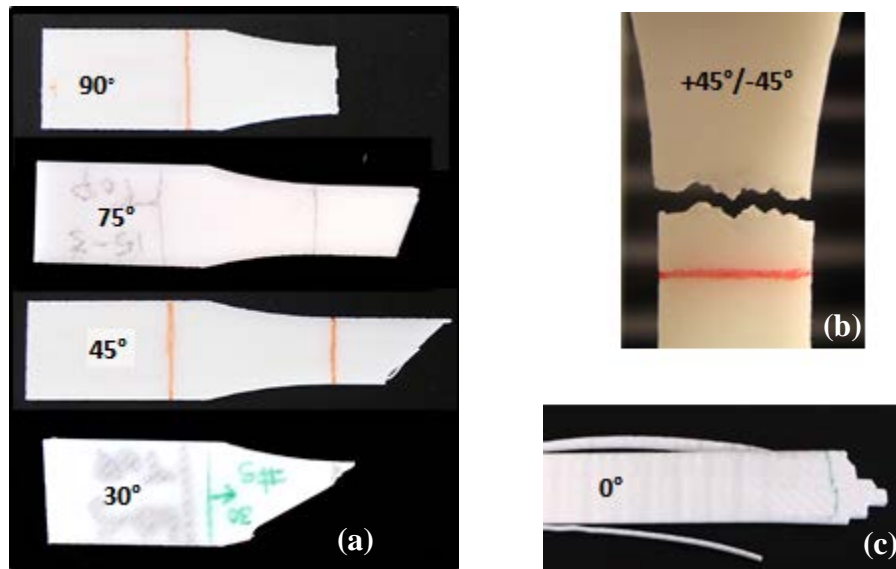


Figure 6. Representative failure modes: (a) specimens failing along the inter-fiber bond, (b) $\theta^\circ/(90-\theta^\circ)$ specimens with intersecting fracture patterns, and (c) 0° specimens with progressive failure from outer width inward.

Also evident in the macroscopic inspection was a degree of obvious stress whitening due to craze formation and growth that developed during deformation in many of the 0° and $\theta^\circ/(90-\theta^\circ)$ specimens. Crazeing generally occurs when localized regions yield, forming an interconnected array of microvoids [15]. Craze bands were seen to form perpendicular to the axis of loading in the tensile and fatigue specimens that experienced the largest amount of deformation prior to fracture. The subsequent failure of these specimens occurred within the whitened crazed areas where some evidence of localized fiber delamination was also observed.

4.2 Microscopic Analysis

SEM analysis of the 0° and $\theta^\circ/(90-\theta^\circ)$ fatigue fractured specimens that displayed obvious crazeing indicated brittle failure with localized micro-shearing on the faces of individual fibers. Several micrographs, such as Figure 7a, displayed evidence of craze formation on the fiber surfaces normal to the loading axis. In contrast, the specimens with $45^\circ \leq \theta \leq 90^\circ$ did not display any obvious crazeing in the macroscopic inspection, and SEM analysis indicated fracture occurred at the weak fusion bond between the layered ABS fibers (Figure 7b). This result

corresponds to the lack of plastic straining evidenced in the analysis of the stress-strain curves associated with the $45^\circ \leq \theta \leq 90^\circ$ orientations, as well as the significantly smaller amount of total plastic extension that occurred in these specimens during fatigue cycling.

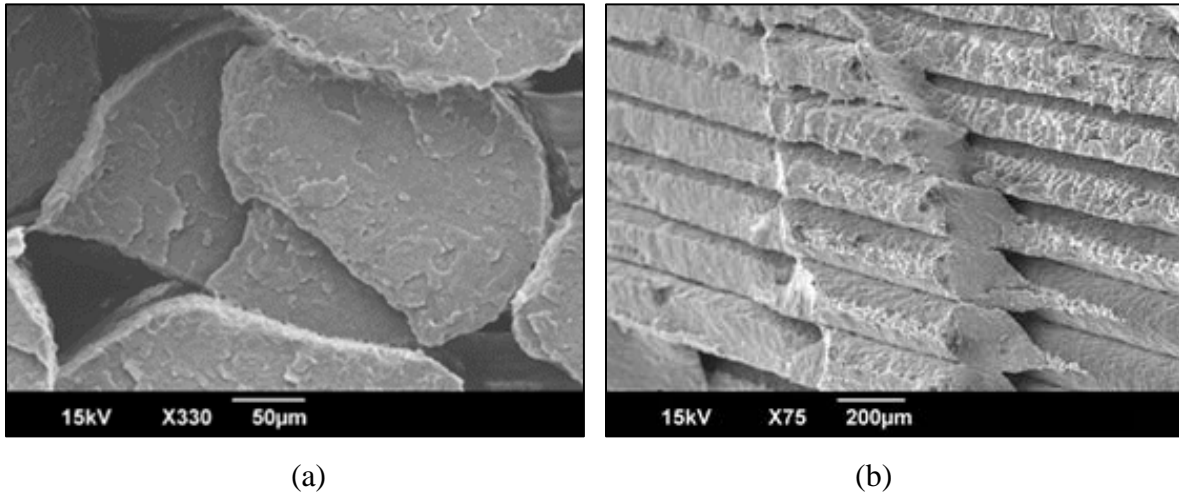


Figure 7. SEM images of fatigue fracture surfaces for (a) $\theta = 0^\circ$ [16] and (b) $\theta = 45^\circ$ rasters.

Figure 8 displays the force-extension plots of two representative specimens, formed during fatigue cycling, in which the plastic extension in the 0° specimen (with obvious crazing) is ultimately more than 4.5 times greater than that in the 45° specimen. The $45^\circ \leq \theta \leq 90^\circ$ specimens also displayed significant reductions in strength and fatigue performance, and experienced brittle interface fracture.

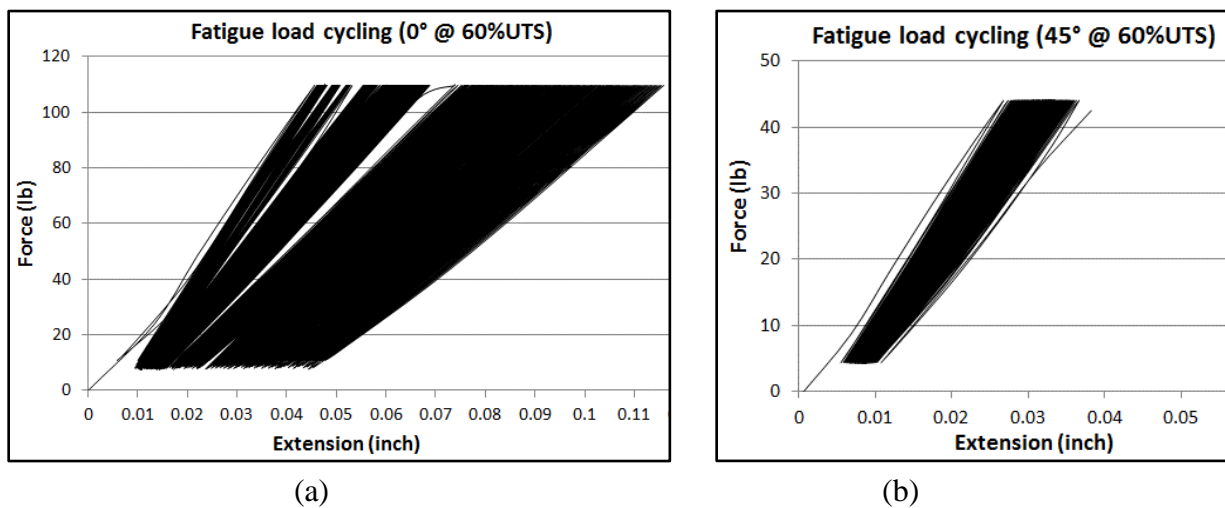


Figure 8. Force-extension plots for two representative tensile-fatigue tests with maximum stress of 60% of UTS. Specimen raster orientations: (a) $\theta = 0^\circ$; (b) $\theta = 45^\circ$;

5. Discussion

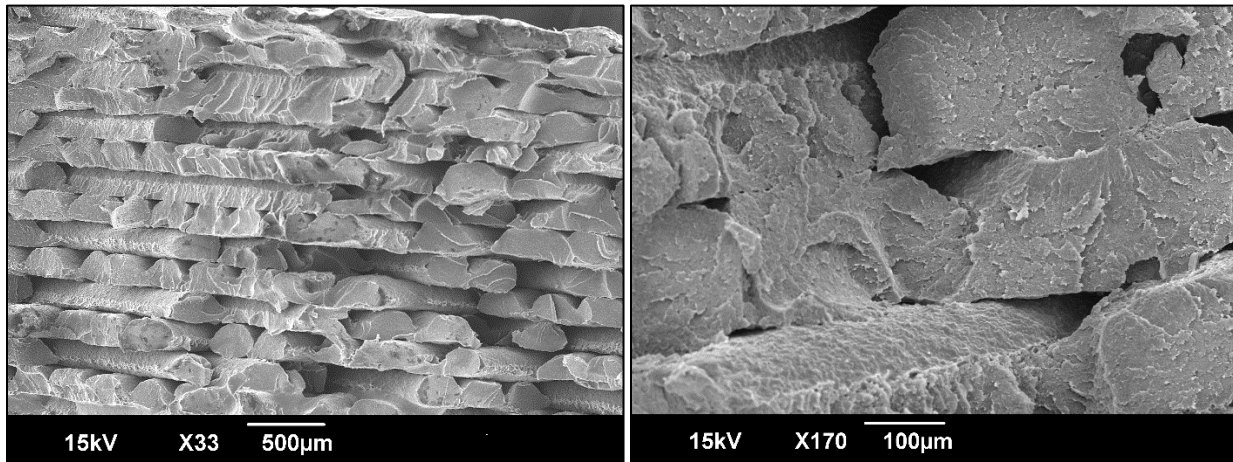
5.1 Inter-fiber Bonds and Air Voids

Data results and macroscopic and microscopic inspection of fractured specimens indicate that the tensile strength and effective stiffness of the unidirectional 0° laminates is greater than that of laminates with fibers running at orientations other than 0° with the stress axis. This result is in agreement with similar tensile studies completed on FDM components [2-5], and is in part due to the strong dependence that the 0° specimen behavior has on the strength and stiffness of the ABS monofilament. The tensile strengths and effective elastic moduli of specimens with fiber orientations of $15^\circ \leq \theta \leq 90^\circ$, in contrast, are adversely affected by the weak fiber-to-fiber fusion strength. Results indicate that the adverse effect of the inter-fiber bond strength increases as the fiber angle, θ , increases from 15° to 90° . In addition to inter-fiber bonding, the strength and stiffness of the FDM specimens are affected by inter-fiber and inter-layer air gaps or voids. Even with the processing *air gap* set to 0.0, the circular nozzle opening and cylindrical shape of the initially extruded fibers cause voids to result within and between the layers of deposited material (as seen in Figure 7a). The effect of these voids amongst the extruded ABS fibers is evidenced by the fact that the mean UTS and effective modulus of the 0° FDM specimens is 9% and 5%, respectively, less than that of the single ABS fiber.

5.2 Alternating Laminae

While the unidirectional 0° rasters achieved the maximum tensile strength and effective elastic modulus of all the FDM specimens, the $+45^\circ/-45^\circ$ specimens survived the largest average number of fatigue cycles to failure at each normalized stress level. Statistical analysis has verified that this difference in the mean number of cycles to failure is significant, indicating that the alternating $\theta^\circ/(90-\theta)^\circ$ layering pattern offers some additional benefit with regard to fatigue life that is not present in the unidirectional raster orientations. It appears that the tendency towards failure along the inter-fiber bonds in the θ direction of a single lamina or layer is consistently counteracted and opposed by the perpendicular $(90-\theta)$ fibers of the adjacent lamina. This counteraction serves to decrease the ease with which a crack can fully propagate through the thickness of the specimen when the maximum stress level is below the UTS. This effect is visible upon inspection of the fracture surface of an alternating $\theta^\circ/(90-\theta)^\circ$, which displays a mixed mode repeated failure of individual fibers by shearing and tension (Figure 9a). Examination of the individual rasters under higher magnification (Figure 9b) reveals failure initiation sites at multiple locations. These pattern variations suggest the possible existence of a dynamic transition of failure mode that is unique to the alternating $\theta^\circ/(90-\theta)^\circ$ raster configurations [16]. The spacing of detectable fatigue striations on the fractured ends of individual fibers may also be an indication of slower crack growth rates.

It is additionally possible that the repeated cycling at a percentage of the mean UTS allows individual fibers to slide with respect to one another and shift position slightly, thereby decreasing the amount of inter-fiber and inter-layer air voids. A decrease in the amount of air gaps within the specimen would make a more difficult fracture path, and thus increase its effective stiffness and strength. This small reorientation would also cause the fibers to be slightly more aligned with the loading direction, causing the strength of each fiber to become relatively more significant.



(a)

(b)

Figure 9. Fracture surface of +45°/-45° fatigue specimen magnified: (a) x33; (b) x170 [16];

5.3 Fatigue Life

Classically, the logarithm of constant amplitude fatigue life, N , is often assumed to be linearly dependent on the logarithm of the governing stress S . This appears to be the case in the current fatigue study as well. The S-N curves in Figure 5 were transformed using the log-base 10 of both the mean number of cycles to failure (N) and the percentage of the UTS defining the maximum stress level per cycle. This transformed data appears as the linear relationships presented in Figure 10. Note that although N is the dependent variable, it is traditionally plotted on the abscissa in graphical representations of S-N curves, as seen in Figure 5. However, Figure 10 shows $\log(N)$ on the ordinate, to more accurately represent the linear relationship that is estimated to determine the fatigue life model parameters.

On the basis of this transformation, the S-N curves of the FDM specimens can be expressed in the classical form of a power law as:

$$N = aS^m$$

where m and a are known as the fatigue exponent and the fatigue coefficient, respectively. In this model, N is the number of cycles to fatigue failure and S is the maximum stress level expressed in %UTS. The material parameters m and a are empirically determined from the experimental fatigue data using a least squares regression fit of $\log(S)$ versus $\log(N)$. The results of the regression analysis appear in Table 4.

In this form, all four curves appear to have somewhat similar decreasing slopes, i.e. parameter m . The positioning of the lines along the horizontal axis of the graph clearly indicates the superior fatigue performance of the 0° and +45°/-45° orientations at each %UTS value, in contrast with the 90° and 45° orientations. Although the tensile strengths and fatigue life of the 90° and 45° raster specimens is significantly smaller than that of the other specimens,

their fatigue life trends as represented by the slopes m in Figure 10 appear very similar to that of the other raster orientations. This appears to suggest that there is some aspect of the cyclical fatigue degradation mechanism that is independent of the printed raster orientation and the UTS of the specimens. Although somewhat surprising, this result is in agreement with the study completed by Lee and Huang [10] and is something that will be considered in future work.

Table 4. Estimated material parameters associated with a power law model for the fatigue life of FDM specimens ($R = 0.10$)

Fiber θ (degrees)	Fatigue Exponent m	Fatigue Coefficient a	R^2
90	-7.67	8.78	0.991
45	-6.62	8.64	0.998
0	-6.40	11.24	0.977
+45/-45	-5.46	9.59	0.994

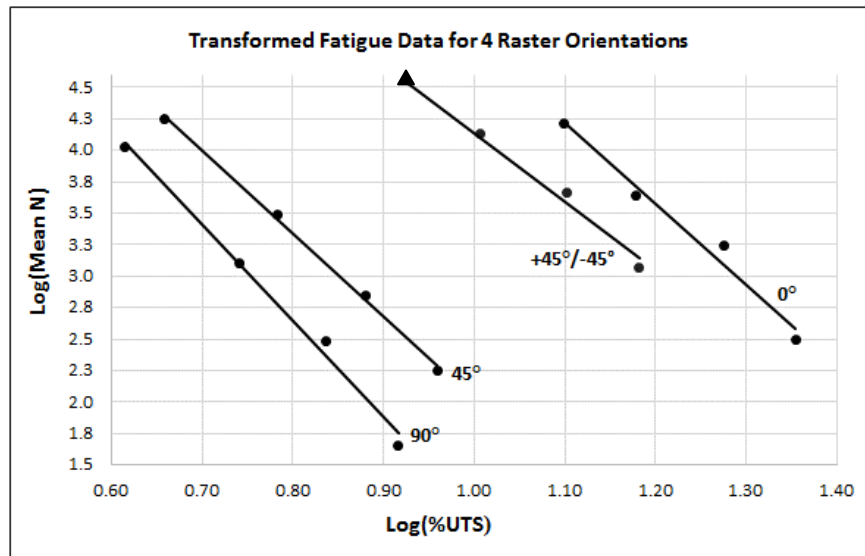


Figure 10. Transformed (log-log) S-N curves for each of the four tested raster orientations, with least squares linear approximation displayed.

Another relevant issue is the differences in the variability of the fatigue data for the studied raster orientations. It should be noted that the amount of scatter in the fatigue data for the 90° and 45° rasters is significantly larger than that for the 0° and +45°/-45° rasters. The standard deviation as a percentage of mean cycle time was computed for each stress level of each raster orientation as a comparable measure of the data variation (Table 5). The significantly larger amount of scatter in the fatigue results for the 90° and 45° orientations is believed to be due to the dependence of these specimens on the inter-fiber bonding, which is a consequence of the manufacturing process. The associated process variability in bond strength is evident in SEM analyses, and serves to add an additional source of variation in fatigue results. In addition, because the interfiber bond is significantly weaker than the ABS monofilament itself, it is likely that any surface imperfections on these specimens will more quickly and significantly affect fatigue life [16]. Because fatigue cracks generally initiate at a surface, the surface condition of

the component being loaded has an effect on its fatigue life. Although great care was taken to ensure that no noticeably defective specimens were used in this study, the variability in fatigue life may indicate that there were some microscopic defects or discontinuities.

Table 5. Variability in fatigue results presented as the standard deviation in cycle time, N , as a percentage of mean cycle time, \bar{N} , for each orientation.

Max % of UTS	Fiber Orientation			
	0°	45°	90°	+45/-45°
90	12.5%	22.6%	30.9%	7.5%
75	9.3%	21.2%	62.8%	8.0%
60	13.7%	28.5%	18.0%	25.4%
45	7.0%	23.7%	26.1%	0.3%
Mean	10.6%	24.0%	34.4%	10.3%

6. Conclusions and Future Work

The monotonic tensile and cyclical tension-fatigue properties of layered FDM specimens display anisotropic behavior and are significantly affected by the both the orientation of the parallel rasters in each lamina, and the pattern of this orientation in successive lamina. The parameter variations appears to most significantly affect the resulting directionality of the polymer molecules, the presence of inter-fiber and inter-lamina air gaps, and the influence of the weaker and somewhat inconsistent inter-fiber fusion bonds, which influence the tensile strength, effective modulus, and fatigue life of these components.

Experimentation and analysis has indicated that the ultimate and yield tensile strengths are the largest and the closest to that of the individual ABS fiber for the unidirectional 0° raster orientation. The primary differences between the individual fiber properties and those of the 0° specimens are the presence of inter-fiber and inter-layer air gaps or voids, and the thermal effects resulting from the melt and deposition during the FDM process. The tensile properties then begin to decrease as the raster angle increases and the specimen behavior becomes more dependent on inter-fiber bonding. The specimens with raster angles of $60^\circ \leq \theta \leq 90^\circ$ suffer the most from the property dependence on the fusion bonds and the decreased relevance of the actual fiber strength. These issues also directly affect the amount of straining that occurs prior to tensile fracture

Tension-tension fatigue results also indicate anisotropic behavior on the basis of raster orientations. The +45°/-45° specimens had the longest fatigue life at each normalized stress level, followed by the 0°, 45°, and 90° orientations in descending order. The difference between the mean number of cycles to failure is statistically significant for all raster orientations at each stress level. Failure modes are similar to those seen in static tension tests.

An interesting result of this study is the superior tension-tension fatigue performance of the alternating +45°/-45° specimens given that the 0° performed the best in static tension tests. Additional research is planned to more thoroughly analyze the cyclical fatigue degradation mechanism in this regard. Work is planned study the fatigue life of other $\theta^\circ/(90-\theta^\circ)$ specimens in an effort to more fully understand the underlying reasons for the improved cyclical performance of the +45°/-45° specimens.

References

- [1] Caulfield, B., McHugh, P. and Lohfeld, S. (2007), Dependence of mechanical properties of polyamide components on build parameters in the SLS process, *Journal of Materials Processing Technology*, Vol. 182, pp. 477–488.
- [2] Rodriguez, J., Thomas, J. & Renaud, J. (2001), Mechanical Behavior of Acrylonitrile Butadiene Styrene (ABS) Fused Deposition Materials. Experimental Investigation. *Rapid Prototyping Journal*, Vol. 7, No. 3, pp. 148-158.
- [3] Rodriguez, J., Thomas, J. and Renaud, J. (2003), Mechanical behavior of acrylonitrile butadiene styrene fused deposition materials modeling, *Rapid Prototyping Journal*, Vol. 9, No. 4, pp. 219-230.
- [4] Ahn, S., Montero, M., Odell, D., Roundy, S. and Wright, P. (2002), Anisotropic Material Properties of Fused Deposition Modeling ABS, *Rapid Prototyping Journal*, Vol. 8, No. 4, pp. 248 –257.
- [5] Sood A., Ohdar R. and Mahapatra, S. (2010), Parametric appraisal of mechanical property of fused deposition modelling processed parts, *Materials and Design*, Vol. 31, No. 1, pp. 287–95.
- [6] Sood, A., Ohdar, R. & Mahapatra, S. (2011). Experimental investigation and empirical modeling of FDM process for compressive strength improvement. *Journal of Advanced Research*, DOI:10.1016/j.jare.2011.05.001.
- [7] Lee, B., Abdullah, J. & Khan, Z. (2005). Optimization of rapid prototyping parameters for production of flexible ABS object. *Journal of Materials Processing Technology*, Vol. 169, pp.54–61.
- [8] Es Said, O., Foyos, J., Noorani, R., Mendelson, M., Marloth, R. and Pregger, B. (2000), Effect of layer orientation on mechanical properties of rapid prototyped samples, *Materials and Manufacturing Processes*, Vol. 15, No. 1, pp. 107–22.
- [9] Ziemian, C., Sharma, M., Ziemian, S. (2012), “Anisotropic Mechanical Properties of ABS Parts Fabricated by Fused Deposition Modelling”, In: *Mechanical Engineering*, Dr. Murat Gokcek (Ed.), ISBN: 978-953-51-0505-3, InTech.
- [10] Lee, J. and Huang, A. (2013), Fatigue analysis of FDM materials, *Rapid Prototyping Journal*, Vol. 19, No. 4, pp. 291-299.
- [11] ASTM Standard D638 - 10. (2010). *Standard Test Method for Tensile Properties of Plastics*. ASTM International, West Conshohocken, Pennsylvania, DOI: 10.1520/D0638-10, Available from: <www.astm.org>
- [12] ASTM Standard D7791 - 12. (2012). *Standard Test Method for Uniaxial Fatigue Properties of Plastics*. ASTM International, West Conshohocken, Pennsylvania, DOI: 10.1520/D7791-12, Available from: <www.astm.org>
- [13] Montgomery, D. (2009), *Design and Analysis of Experiments* (7th Edition), John Wiley and Sons, ISBN 978-0-470-12866-4, Hoboken, New Jersey
- [14] Sun, Q., Rizvi, G., Bellehumeur, C. and Gu, P. (2008), Effect of processing conditions on the bonding quality of FDM polymer filaments, *Rapid Prototyping Journal*, Vol. 14, No. 2, pp. 72 – 80.

- [15] Mae, H., Omiya, M., Kishimoto, K. (2008), Tensile Behavior of Polypropylene Blended with Bimodal Distribution of Styrene-Ethylene-Butadiene-Styrene Particle Size, *Journal of Applied Polymer Science*, Vol. 107, pp. 3520–3528.
- [16] Ziemian, S., Okwara, M., Ziemian, C. (2015). Tensile and Fatigue Behavior of Layered Acrylonitrile Butadiene Styrene, *Rapid Prototyping Journal*, to appear in Vol. 21, No.4.